THE JOURNAL OF PHYSICAL CHEMISTRY C

Article

Cite This: J. Phys. Chem. C 2019, 123, 14849−14857

pubs.acs.org/JPCC

Ultraviolet Light-Induced Degradation of Luminescence in Mn-Doped $CsPbCl_3$ Nanocrystals

Qiuyan Li,[†] Sihang Ji,[†] Xi Yuan,*[,†] Ji Li,[†] Yi Fan,[‡] Jiahua Zhang,[‡] Jialong Zhao,[†,§,∥] and Haibo Li*[,†,§]

[†]Key Laboratory of Functional Materials Physics and Chemistry of the Ministry of Education, Jilin Normal University, Changchun 130103, P. R. China

[‡]State Key Laboratory of Luminescence and Applications, Changchun Institute of Optics, Fine Mechanics and Physics, Chinese Academy of Sciences, Changchun 130033, P. R. China

[§]Key Laboratory of Preparation and Application of Environmental Friendly Materials, Ministry of Education, Jilin Normal University, Changchun 130103, P. R. China

[∥]National Demonstration Center for Experimental Physics Education, Jilin Normal University, Siping 136000, P. R. China

Supporting Information

ABSTRACT: Improving the photostability of highly luminescent Mn^{2+} doped all-inorganic halide perovskite nanocrystals (NCs) is challenging because their excellent optical performances are determined by the stable structure and low defect/trap states. The optical properties of Mn^{2+} doped $CsPbCl_3$ (Mn^{2+}:$CsPbCl_3$) NCs with various Mn^{2+} doping concentrations under ultraviolet (UV) illumination were studied to unravel their photodegradation by using photoluminescence (PL) spectroscopy at room temperature. The PL intensities of band-edge excitons and Mn^{2+} ions in the Mn^{2+}:$CsPbCl_3$ NC films significantly decreased due to formation of nonradiative defects/traps in NCs with increasing illumination times. It was surprisingly found that the single- and multiexponential decay times (1.81−1.15 ms) of Mn^{2+} emissions ranging from 595 to 640 nm observed in the doped NC films with low and high Mn/Pb ratios were almost not varied with increasing UV illumination times. However, the blue-shift of Mn^{2+} emission was observed in high Mn^{2+} doping concentration NCs under illumination, which might result from the diffusion of Mn^{2+} ions to the surface of doped NCs. Further, the surface passivation of Mn^{2+}:$CsPbCl_3$ NCs by using a Cs_4PbCl_6 shell was found to effectively suppress the photodegradation of Mn^{2+}:$CsPbCl_3$ NCs and enhance the PL stability of Mn^{2+}.

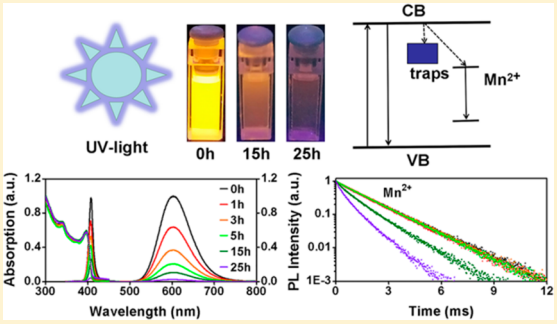

1. INTRODUCTION

The metal halide perovskite nanocrystals (NCs) with tunable photoluminescence (PL) wavelengths and high PL quantum yields (QYs) have shown practical applications in solar cells, light-emitting diodes (LEDs), and lasers.[1−13] A new kind of nanophosphor successfully achieved by doping manganese ions (Mn^{2+}) into perovskites such as $CsPbCl_3$ NCs in 2016 provide a bright orange−red Mn^{2+} emission around 586−600 nm.[14,15] It is known that the broad orange emissions of Mn^{2+} doped $CsPbCl_3$ (Mn^{2+}:$CsPbCl_3$) NCs are attributed to the Mn^{2+} $^4T_1 \rightarrow {}^6A_1$ d−d transition by energy transfer from excitons in the $CsPbCl_3$ host to Mn^{2+} dopants.[14−30] Further, the emission wavelengths of Mn^{2+} in $CsPbCl_3$ NCs can be tuned from 580 to 620 nm by changing the Mn^{2+} doping concentration from low to high, which is attributed to formation of Mn^{2+}−Mn^{2+} dimers or defects at higher Mn^{2+} doping level.[14−16,23,24] The highly luminescent yellow−red emitting phosphors have been used for fabricating white light-emitting devices with a UV lamp excitation of 365 nm or a blue GaN chip.[30−33] Therefore, it is necessary to understand the UV light-induced degradation of luminescence in Mn^{2+}:$CsPbCl_3$ NCs in ambient air to improve their photostability.

The stability of lead halide perovskites is not very high, and they are chemically unstable when they are exposed to light and heat because of the low formation energies.[34−41] The light illumination-induced degradation was attributed to decomposition of methylammonium lead halide perovskite.[37−41] Recently, the light-induced degradation of $CsPbBr_3$ NCs under high-power LED illumination was also studied, and the PL reduction was related to oxygen-induced degradation and increased surface trap states due to growth of NCs.[42] Further the spectroscopic and structural studies verified that light illumination led to detachment of the capping agent, collapse of the $CsPbI_3$ NC surface, and aggregation of surface Pb atoms.[43] Therefore, the light-induced structural variation would result in formation of defects/trap states in NCs,

Received: April 9, 2019
Revised: May 20, 2019
Published: May 23, 2019

DOI: 10.1021/acs.jpcc.9b03294
J. Phys. Chem. C 2019, 123, 14849−14857

seriously degrading the optoelectronic properties and performances of perovskite NCs and their related devices.

The improved and extended luminescent properties of $CsPbCl_3$ NCs have been demonstrated by doping metal and rare earth ions such as Mn, Ni, Cd, Yb, and so on into $CsPbCl_3$ NC host.[14−16,44−52] Especially considerable improvement in exciton emissions and optical stabilities in $CsPbCl_3$ NCs was considered to result from doping-enhanced short-range structural order and effective surface passivation of NCs.[47−52] The high structural and optical stabilities were also observed in Mn^{2+} doped $CsPbBr_3$ and $CsPbI_3$ NCs.[53,54] The rational metal doping has been considered to be a useful strategy for improving the PL quantum yields and photostabilities of perovskite NCs and related devices.[55−57] It is noteworthy that efficient Mn^{2+} luminescence has been observed from $CsPbCl_{3-x}Br_x$ NCs of varied size and composition.[14,15] In particular, it is surprisingly found that the Mn^{2+} emissions in the doped NCs with low dopant concentration in solution exhibited nearly size-independent and single-exponential decay lifetimes of up to 1.8 ms at room temperature.[23,58] Therefore, studying the optical properties of Mn^{2+}:$CsPbCl_3$ NCs under ultraviolet (UV) light illumination will help one better understand the variation and control in optical stability of doped NCs.

In this work, the optical properties of Mn^{2+}:$CsPbCl_3$ NCs with various Mn^{2+} doping concentrations under UV illumination are studied to unravel their photodegradation processes using photoluminescence (PL) spectroscopy at room temperature. The reduction in PL intensities of band-edge excitons and Mn^{2+} ions was observed in the Mn^{2+}:$CsPbCl_3$ NCs due to formation of nonradiative defects/traps with increasing illumination times. The almost unchanged single- and multiexponential decay times of Mn^{2+} emissions ranging 595 to 640 nm observed in the doped NC films with low and high Mn/Pb ratios were found with increasing UV illumination times. It is worth noting that we observed the blue-shift of Mn^{2+} emission wavelength in high Mn^{2+} concentration doped NC films due to the diffusion of Mn^{2+} ions to the surface of doped NCs. Further a Cs_4PbCl_6 shell was used to enhance the PL stability of Mn^{2+} ions in Mn^{2+}:$CsPbCl_3$ NCs.

2. EXPERIMENTAL SECTION

2.1. Materials. Cesium carbonate (Cs_2CO_3, 99.99%, Alfa Aesar), manganese chloride ($MnCl_2$, 99.99%, Alfa Aesar), lead chloride ($PbCl_2$, 99.999%, Alfa Aesar), 1-octadecene (ODE, 90%, Alfa Aesar), trioctylphosphine (TOP, 90%, Aldrich), oleylamine (OLA, 70%, Aldrich), oleic acid (OA, 90%, Aldrich), and hexane (98%, Beijing Chemical Works) were purchased. All reagents were used without further purification.

2.2. Preparation of Cesium Oleate Solution. The Cs_2CO_3 (0.68 mmol) was mixed with OA (0.65 mL) and ODE (10 mL), loaded into a 50 mL three neck round-bottom flask, and degassed under vacuum at 110 °C for 30 min. Then the mixed solution was heated up to 150 °C for at least 15 min under the protection of argon, until a clear solution was obtained.

2.3. Synthesis of Mn^{2+}:$CsPbCl_3$ NCs. The Mn^{2+}:$CsPbCl_3$ NCs were synthesized by modifying a prior report.[23,58] Typically, $MnCl_2$ (0.2 mmol) and $PbCl_2$ (0.2 mmol) were loaded together along with ODE (5 mL), OA (1.2 mL), OLA (1.2 mL), and TOP (1 mL) in a 50 mL three neck round-bottom flask. After being stirred and degassed under vacuum at 110 °C for 30 min, the reaction mixture was heated up to 190 °C under argon flow. Then, the hot cesium oleate solution (0.25 mL) was swiftly injected and stirred for 15 s at that temperature. The solution was cooled in an ice-water bath to quench the reaction.

The Mn doped $CsPbCl_3$ NCs with varied dopant concentrations were prepared by varying the molar feed ratio of $PbCl_2$/$MnCl_2$ and keeping the total molar amount of Pb^{2+} and Mn^{2+} unchanged. The Mn doped $CsPbCl_3$ NCs with various particle sizes were prepared by controlling the reaction temperature as well as the amounts of OA and OLA. For the small (4.36 ± 0.23 nm), medium (8.82 ± 0.71 nm), and large (15.11 ± 1.52 nm) NCs, the reaction temperatures were 170, 190, and 210 °C, respectively, and were accompanied by an increase in the amounts of OA and OLA.

2.4. Synthesis of Mn^{2+}:$CsPbCl_3$/Cs_4PbCl_6 Core/Shell NCs. After the as-prepared Mn^{2+}:$CsPbCl_3$ NCs were immersed in ice-water bath, $ZnCl_2$ (1.15 mmol) was loaded together with the as-prepared Mn^{2+}:$CsPbCl_3$ NC solution. After being stirred under vacuum at 50 °C for 25 min, the solution was heated up to 75 °C under argon flow. Then, the hot cesium oleate solution (1 mL) was swiftly injected and stirred for 1 min. The solution was cooled in an ice-water bath to quench the reaction. The produced Mn^{2+}:$CsPbCl_3$/Cs_4PbCl_6 core/shell NCs were centrifuged at 5000 rpm for 7 min, and the final precipitate was dispersed in hexane.

2.5. Characterization. Ultraviolet−visible (UV) absorption spectra were recorded on a Shimadzu UV-2700 spectrophotometer. Steady-state and time-resolved PL spectra were collected using a Horiba Jobin Yvon Fluorolog-3 spectrofluorometer, with a continuous 450 W xenon lamp as excitation source for PL spectra and a N-305 Nano LED and xenon flash tube as excitation source for PL decay measurement of exciton and Mn^{2+}, respectively. PL QYs were recorded via an Otsuka QE-2000. Transmission electron microscopy (TEM) was taken on a JEOL-JEM-2100 microscope. X-ray diffraction (XRD) patterns carried out in Rigaku D/max-2500 diffractometer with Cu Kα radiation (λ = 1.54 Å) as the incident radiation. Mn-doping concentration was determined using inductively coupled plasma mass spectrometry (ICP-MS, PerkinElmer Nexion350-X). The UV illumination light came from a lamp (6 mW, ZF-7, Shanghai Jiapeng Technology). For UV illumination measurement, thin NC solid films were prepared via spin-coating the purified NC solution on silicon wafer substrates. The thicknesses of Mn^{2+}:$CsPbCl_3$ and Mn^{2+}:$CsPbCl_3$/Cs_4PbCl_6 NC films were estimated to be 12−32 and 30−62 nm, respectively, by an optical thickness meter (OPTM-A1, Otsuka Electronics).

3. RESULTS AND DISCUSSION

The luminescence properties of the colloidal Mn^{2+}:$CsPbCl_3$ NCs in solution and in solid films under 365 nm UV lamp illumination were evaluated in detail to understand their photostability. Figure 1a shows the absorption and PL spectra of Mn^{2+}:$CsPbCl_3$ NCs in hexane at various illumination times at room temperature. The initial PL QY of the Mn^{2+} doped $CsPbCl_3$ NCs without UV illumination is 61.1% ± 4.5%. The exciton absorption band is peaked at 400 nm. The PL peak wavelengths of band-edge excitons and Mn^{2+} ions for colloidal Mn^{2+}:$CsPbCl_3$ NCs are 403 nm with a full width at half-maximum (fwhm) of 11 nm (83 meV) and 600 nm with a fwhm of 85 nm (291 meV), respectively, consistent with the observation in previous reports.[14,15] No clear change in absorption spectra is observed after long-time illumination;

DOI: 10.1021/acs.jpcc.9b03294
J. Phys. Chem. C 2019, 123, 14849−14857

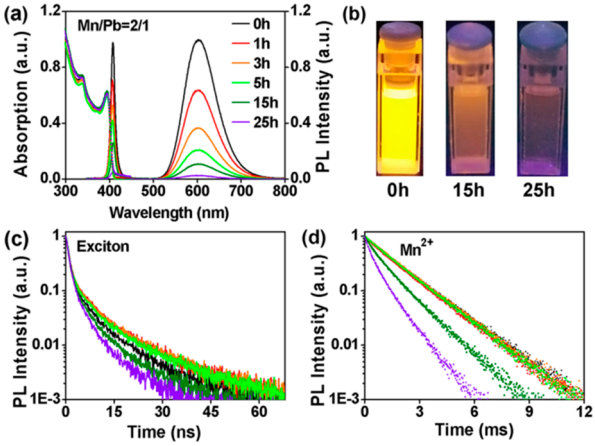

Figure 1. Absorption (dot lines) and PL spectra (solid lines) of Mn^{2+}:$CsPbCl_3$ NCs with a Mn/Pb molar ratio of 2/1 in hexane (a), digital photos of the NC solution in a cuvette (b), and band-edge PL and Mn^{2+} emission decay curves (c, d) under various UV illumination times.

however, both the PL intensities from band-edge excitons and Mn^{2+} ions significantly decrease and are apparently quenched after 25 h illumination time. It is noted that the band-edge exciton PL has a peak red-shift of 8 nm while the Mn^{2+} ion emission does not have any peak red-shift. Figure 1b shows the digital photos of a Mn^{2+}:$CsPbCl_3$ NC sample at different illumination times. The Mn^{2+}:$CsPbCl_3$ NC solution initially has a strong yellow color, and it turns very dark after 25 h. Figure 1c and d shows the PL decay curves of band-edge excitons and Mn^{2+} ions in Mn^{2+}:$CsPbCl_3$ NC sample. The average PL lifetimes were estimated using eq 1,[59]

$$\tau_{av} = \frac{\sum_i A_i \tau_i^2}{\sum_i A_i \tau_i} \quad (1)$$

where A_i and τ_i are the weights and time components of the exponential function used to fit the PL decay curves. The initial PL decay time of band-edge excitons is 4.31 ± 0.05 ns. It becomes slightly longer to 8.28 ± 0.11 ns with increasing illumination time and then turns shorter to 2.80 ± 0.03 ns. On the other hand, the PL decay time of Mn^{2+} ions initially is kept a constant, which is 1.81 ± 0.02 ms, within 5 h illumination time, and then it turns shorter to 0.77 ± 0.07 ms after 25 h illumination. The reduction in the PL intensity for band-edge excitons and Mn^{2+} ions is attributed to formation of defects/traps in the doped NCs.[42] The observation of red-shift in band-edge PL and shortening of Mn^{2+} PL lifetimes also demonstrate the aggregation or growth of NCs after long UV illumination.[42,58,60] The TEM images of the Mn^{2+}:$CsPbCl_3$ NCs without/with 25 h illumination time were measured as shown in Figure S1a and b. The sample has quite uniform NCs with average size of ~8.82 ± 0.71 nm before illumination, while it has aggregated NCs in the size range of 20 nm after 25 h illumination. To avoid the complex photodegradation mechanism of colloidal Mn^{2+}:$CsPbCl_3$ NC solution due to the growth of NCs, the Mn^{2+}:$CsPbCl_3$ NC films on silica substrates are used to study their photostability.

The luminescence properties of Mn^{2+}:$CsPbCl_3$ NCs with various sizes under UV illumination are studied. The NC samples with exciton PL peaks at 390, 403, and 406 nm are called NC390, 403, and 406, respectively, and they were synthesized with the same Mn/Pb ratio of 2/1 by varying reaction temperature and ligand amount. The Mn^{2+} doped NC samples have average NC sizes of 4.36 ± 0.23, 8.82 ± 0.71, and 15.11 ± 1.52 nm, respectively, as shown in Figure S1c and d. The Mn^{2+} ion emissions in these doped NCs are at ~600 nm, meaning that the PL is from isolated Mn^{2+} ions due to low dopant concentration.[14,15,22−24] The PL spectra of Mn^{2+}:$CsPbCl_3$ NC films for NC390, 403, and 406 samples under UV illumination for various times are shown in Figure 2a and b and Figure S2a. It is observed that the PL intensities

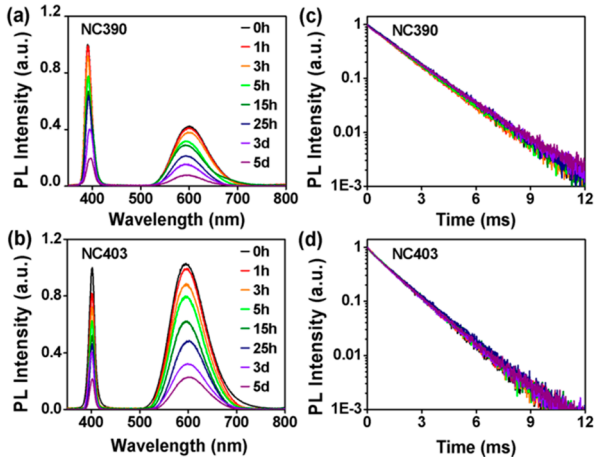

Figure 2. PL spectra and Mn^{2+} emission decay curves of Mn^{2+}:$CsPbCl_3$ NC films for NC390 (a, c) and 403 (b, d) under UV lamp illumination at various times.

of band-edge excitons and Mn^{2+} ions clearly decrease with increasing illumination time, indicating the photoinduced degradation of the doped NCs due to the formation of nonradiative defects/traps in the NC hosts. The exciton PL for the smallest NC390 slightly shifts to the long wavelength, perhaps due to aggregation of NCs, while it is kept a constant for the larger-sized NC403 and 406, perhaps meaning that the NC sizes do not have a clear change, in agreement with the TEM images before and after 120 h illumination as seen in Figure S3a and b. The XRD patterns of NC406 after being illuminated for different times are shown in Figure S3c; the diffraction patterns are basically unchanged, which proves that the main lattice structure of the NCs is retained during illumination. The Mn^{2+} emission decay curves of Mn^{2+}:$CsPbCl_3$ NC films for NC390, 403, and 406 under UV lamp illumination at various times are shown in Figure 2c and d and Figure S2b. In contrast to significantly reduced lifetimes of band-edge excitons as seen in Figure S4, no change in Mn^{2+} emission decay curves is clearly observed for NC390, 403, and 406.

Figure 3 shows the PL intensities and lifetimes of band-edge excitons and Mn^{2+} ions in the Mn^{2+}:$CsPbCl_3$ NC films as a function of illumination time. The decrease in PL intensities of band-edge excitons and Mn^{2+} ions for these doped NCs is significant under UV illumination for the first 15 h and then becomes slow, and the PL intensity almost is quenched after illumination of 120 h. The PL lifetimes of band-edge excitons for three doped NC samples slightly increase after 15 h illumination and then gradually decrease with increasing illumination time. As seen in Figure 3c, the reduction trend of band-edge PL lifetimes is quite different from that of their PL intensities, suggesting that the band-edge PL may originate not only from exciton recombination but also from other kinds

DOI: 10.1021/acs.jpcc.9b03294
J. Phys. Chem. C 2019, 123, 14849−14857

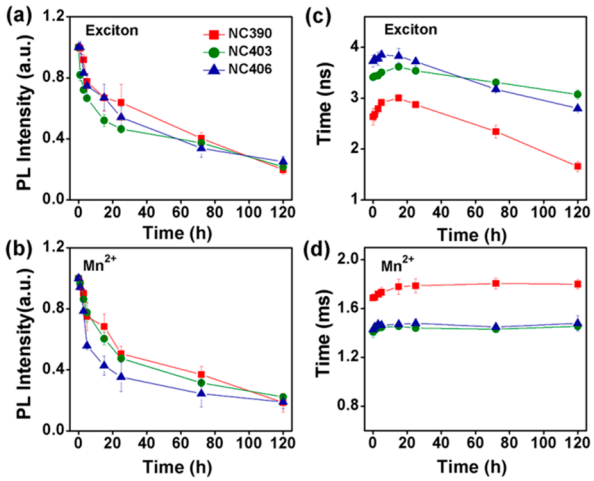

Figure 3. PL intensities and lifetimes of band-edge excitons (a, c) and Mn^{2+} ions (b, d) in the Mn^{2+}:$CsPbCl_3$ NC films as a function of illumination time. The PL intensities are normalized for their initial samples without UV illumination.

of recombination centers.[61] Further, it is surprisingly found that the PL lifetimes of Mn^{2+} ions for NC390, 403, and 406 without UV illumination are 1.68 ± 0.01, 1.45 ± 0.04, and 1.40 ± 0.01 ms, respectively; the PL lifetimes have a slight increase within the first 15 h and then almost remain constant, even after being illuminated for a long time of 120 h. It has been reported that the PL lifetimes of Mn^{2+} ions in Mn^{2+}:$CsPbCl_3$ NCs are significantly varied when their sizes grow due to heat-induced structural change around Mn^{2+} ions.[58] The illumination effect on the size of doped NCs is very weak here because of the low power (6 mW) of the UV365 lamp used in this experiment. This indicates that the local environment of Mn^{2+} ions is not changed too much, attributed to relatively stable Mn−Cl bonds and no efficient energy transfer between Mn^{2+} ions and newly formed defects/traps in the NC hosts.[62]

The PL spectra and Mn^{2+} emission decay curves of Mn^{2+}:$CsPbCl_3$ NC films with Mn/Pb molar ratios of 1/1, 3/1, and 5/1 under UV illumination at various times are shown in Figure 4. The Mn^{2+} doping concentrations and PL QYs of

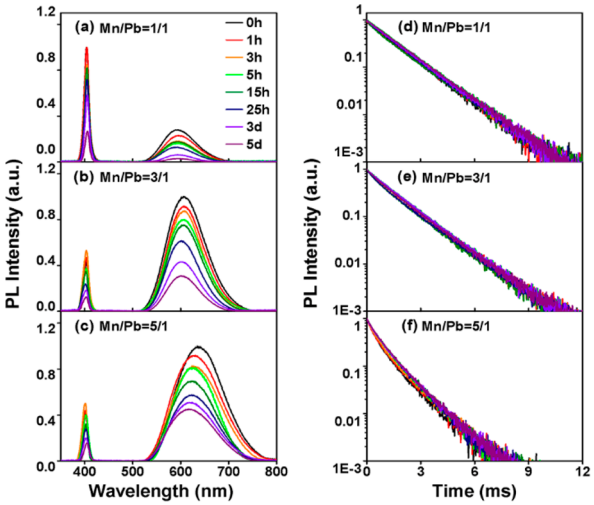

Figure 4. PL spectra and Mn^{2+} emission decay curves of Mn^{2+}:$CsPbCl_3$ NC films with Mn/Pb molar ratios of 1/1 (a, d), 3/1 (b, e), and 5/1 (c, f) under UV illumination at various times.

these Mn^{2+}:$CsPCl_3$ NCs are summarized in Tables S1 and S2. For the Mn^{2+} doped NC film with a Mn/Pb molar ratio of 1/1, its PL intensities for band-edge excitons and Mn^{2+} ions (PL peak at 595 nm) decrease significantly with increasing UV illumination time. The Mn^{2+} PL peak does not have a clear shift, while its PL decay curve shows a perfect single-exponential decay that is almost not related to illumination time. For the Mn^{2+} doped NC film with a Mn/Pb molar ratio of 3/1, its PL intensities for band-edge excitons and Mn^{2+} ions (PL peak at 610 nm) reduce significantly with increasing UV illumination time, and its Mn^{2+} PL peak has a small blue-shift of several nanometers. The red-shift of Mn^{2+} ions from 595 to 620 nm is related to formation of Mn^{2+}−Mn^{2+} pairs due to the increased Mn doping concentration.[23,24,63−65] In addition, its PL decay curve is not single-exponential initially and seems to become single-exponential with increasing illumination time.[23,24,63−65] For the Mn^{2+} doped NC film with a Mn/Pb molar ratio of 5/1, its PL intensities for band-edge exciton and Mn^{2+} ions with an emission of 640 nm decrease obviously with increasing UV illumination time, and its Mn^{2+} PL peak has a large blue-shift of >15 nm. In addition, its decay curve is a multiexponential initially and becomes slightly slow with increasing illumination time.

Figure 5 shows the PL intensities, peak wavelengths, and lifetimes of Mn^{2+} ions in $CsPbCl_3$ NCs with various Mn/Pb

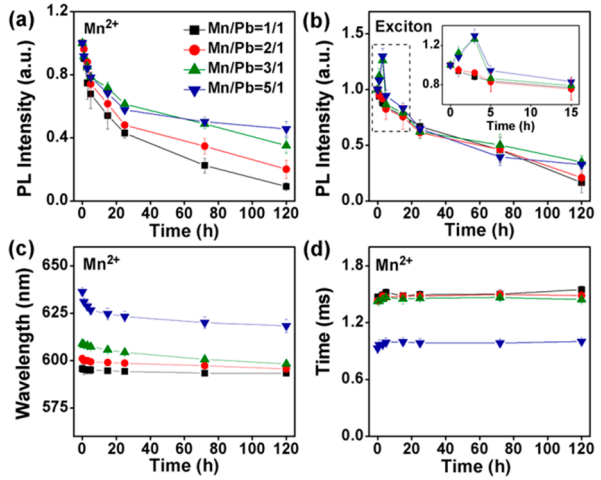

Figure 5. PL intensities of Mn^{2+} ions (a) and band-edge exciton (b), PL peak wavelengths (c), and PL lifetimes (d) of Mn^{2+} in Mn^{2+}:$CsPbCl_3$ NCs with various Mn/Pb ratios as a function of UV illumination times. The inset in (b) shows an enlarged PL intensity dependence on the illumination time.

ratios as a function of UV illumination times. For comparison, the illumination time dependence of band-edge PL intensities is shown in Figure 5b. As seen in Figure 5a, it is observed that the PL intensities of Mn^{2+} ions in the doped NCs significantly decrease with increasing illumination times. For the initial 15 h, the reduction of PL intensities is rapid and becomes gradually slower with increasing illumination time to 120 h. In particular, the PL intensities of Mn^{2+} ions in doped NCs with high Mn/Pb ratios of 3/1 and 5/1 show a relatively slow reduction, compared with those of the other two NC samples with low Mn/Pb ratios of 1/1 and 2/1, meaning that the Mn^{2+}:$CsPbCl_3$ NCs with high Mn doping concentration are more stable. As seen in Figure 5b, for the doped NCs with low Mn/Pb ratios of 1/1 and 2/1, the PL intensities of Mn^{2+} ions

DOI: 10.1021/acs.jpcc.9b03294
J. Phys. Chem. C 2019, 123, 14849−14857

with emissions of 595 and 600 nm clearly decrease with illumination time while those of Mn^{2+} ions with emissions of 610 and 640 nm increase within the initial 3 h, which is clearly seen in the inset of Figure 5b, and then gradually decrease until 120 h. As seen in Figure 5c, for the doped NCs with low Mn/Pb ratios of 1/1 and 2/1, thre Mn^{2+} PL peaks at 595 and 600 nm almost do not change with illumination time. The PL peaks of Mn^{2+} ions at 610 and 640 nm in doped NC films with high Mn/Pb ratio of 3/1 and 5/1 have a clear blue-shift with increasing illumination times, compared to the negligible shift for those NCs with low Mn^{2+} doping concentration. For example, the Mn^{2+} ion emission in doped NCs with the highest Mn/Pb ratio of 5/1 shifts to 620 nm from the initial 640 nm after 120 h illumination. It is noted that the blue-shift of Mn^{2+} emission within the first 15 h is significant. As seen in Figure 5d, it is observed that the doped NCs with high dopant concentration exhibit a significantly reduced Mn^{2+} PL lifetime with increasing Mn/Pb ratio from 3/1 to 5/1. However, the illumination effects on PL lifetimes of Mn^{2+} doped NCs is not significant, even for the high-concentration Mn^{2+} doped NCs. For all the NC films, the Mn^{2+} emissions exhibit a slight rise in PL lifetimes before the first 5 h and do not show a clear change with continually increasing illumination times. For the high Mn^{2+} doping concentration Mn^{2+}:$CsPbCl_3$ QDs with Mn/Pb ratios of 3/1 and 5/1, the observed blue-shift of Mn^{2+} emissions after illumination suggests that Mn^{2+} ions in the NCs diffuse out of doped NCs, resulting in a reduction in numbers of Mn^{2+}−Mn^{2+} pairs, which should in turn enhance the PL intensities and lifetimes of band-edge excitons and Mn^{2+} ions. As seen in Figure 5b, the enhancement of band-edge exciton PL is clearly observed due to reduced energy transfer from $CsPbCl_3$ NC host to Mn^{2+} ions. However, the enhancement of Mn^{2+} emissions, especially the increase in Mn^{2+} PL lifetimes, is not clearly found. It is known that the Mn^{2+} PL QYs and lifetimes in $CsPbCl_3$ NCs with increasing Mn^{2+} doping concentration are reduced due to the increased Mn^{2+}−Mn^{2+} pairs and poor crystallinity.[14,15,23] The diffusion of Mn^{2+} ions in the solid films from inside NCs to the outside NCs does not clearly change the environment around Mn^{2+} ions, because the Mn^{2+} emission decay does not exhibit an obvious change with increasing illumination times, as seen in Figures 4d−f and 5d.

To understand the origin of the blue-shift in Mn^{2+} PL, the PL decay curves of Mn^{2+} ions in $CsPbCl_3$ NC solution and films with various Mn/Pb ratios at different emission wavelengths were measured. The PL decay curves of Mn^{2+} ions in $CsPbCl_3$ NC films with various Mn/Pb ratios of 1/1, 2/1, 3/1, and 5/1 at different emission wavelengths are shown in Figure 6. Figure S5 shows the PL decay curves of Mn^{2+} ions in $CsPbCl_3$ NCs in hexane with various Mn/Pb ratios of 1/1, 2/1, 3/1, and 5/1 at different emission wavelengths. As seen in Figure 6a and b, Mn^{2+} ions in the $CsPbCl_3$ NC films with low Mn/Pb ratios of 1/1 and 2/1 exhibit the same single-exponential PL decay at different emission wavelengths, having the same PL lifetime of 1.41 ± 0.02 and 1.50 ± 0.03 ms, respectively, which are slightly shorter than 1.81 ± 0.01 and 1.76 ± 0.01 ms of those in hexane (Figure S5a and b). The same single-exponential PL decays of Mn^{2+} ions in the $CsPbCl_3$ NC solution at different emission wavelengths were observed in previous reports.[14,15,23,58] This indicates that the environment around the Mn^{2+} ion in the doped NCs with different sizes is the same. As seen in Figure 6c and d, the Mn^{2+} ions in the $CsPbCl_3$ NC films with high Mn/Pb ratios of 3/1

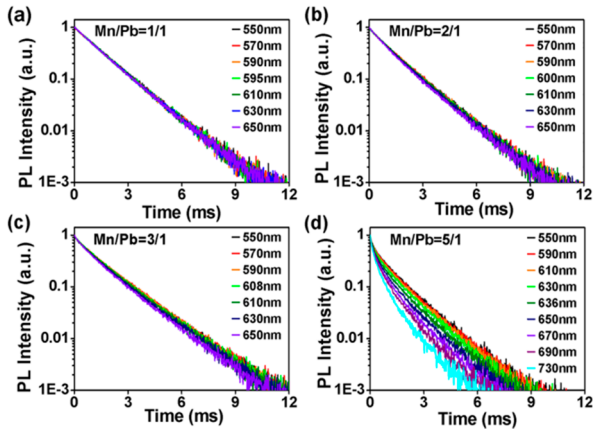

Figure 6. PL decay curves of Mn^{2+} ions in Mn^{2+}:$CsPbCl_3$ NCs with various Mn/Pb ratios of 1/1 (a), 2/1 (b), 3/1 (c), and 5/1 (d) by monitoring different emission wavelengths.

and 5/1 show a multiexponential PL decay at different emission wavelengths, having quite different PL lifetimes, which are strongly dependent on the monitored wavelength. For example, the PL lifetimes of Mn^{2+} ions in the NC film with high Mn/Pb ratios of 3/1 and 5/1 dramatically decrease to 1.42 ± 0.02 and 0.63 ± 0.04 ms from 1.55 ± 0.03 and 1.20 ± 0.05 ms, respectively, at their PL peak wavelengths when the monitored emission wavelength is changed from 550 to 650 nm for the doped NCs with Mn/Pb ratios of 3/1 and from 550 to 730 nm for the doped NCs with a Mn/Pb ratio of 5/1, as shown in Figure 6c and d. Meanwhile, those in hexane are only reduced to 1.64 ± 0.01 and 1.04 ± 0.04 ms from 1.69 ± 0.02 and 1.29 ± 0.01 ms, as seen in Figure S5c and d. The PL lifetimes of Mn^{2+} emissions are 1.68 ± 0.01 and 1.13 ± 0.02 ms (in hexane) and 1.54 ± 0.04 and 1.01 ± 0.06 ms (in films) at their peak wavelengths at 610 and 642 nm (in hexane) and 608 and 636 nm (in films), respectively, for $CsPbCl_3$ NCs with high Mn/Pb ratios of 3/1 and 5/1. Compared with the Mn^{2+} doped $CsPbCl_3$ NCs in hexane, the significant reduction in the PL lifetimes of NCs in films is probably because that the local environment of Mn^{2+} ions in NCs is changed during the film preparation by spin-coating. The wide distribution of PL lifetimes in NC films observed at different emission wavelengths as shown in Figure 6d is not attributed to energy transfer from small NCs to large ones because there is no spectral overlapping between the Mn^{2+} emission and NC absorption.[62] This is attributed to the size distribution of the doped NCs with high Mn^{2+} doping concentration. The corresponding TEM images of Mn^{2+}:$CsPbCl_3$ NCs with Mn/Pb ratios of 5/1 are shown in Figure S6a. The average size of the NCs is 8.38 ± 1.93 nm, which shows a large size distribution from 4.12 to 13.61 nm, as seen in Figure S6b. The small- and large-sized NCs may have different numbers of Mn^{2+}−Mn^{2+} pairs and defect/trap states, perhaps resulting in a significant difference in PL lifetimes of Mn^{2+} ions in NC films when the monitored Mn^{2+} emission wavelength is varied. The true origin is unknown. Therefore, the reduction in PL lifetime of Mn^{2+} ions indicates the naked Mn^{2+}:$CsPbCl_3$ NCs are not stable in size and structure during film preparation.

Further, to improve the photostability of the doped NCs, the Mn^{2+}:$CsPbCl_3$ NCs were coated with a Cs_4PbCl_6 shell by following a previous method.[66] The TEM images and XRD patterns of Mn^{2+}:$CsPbCl_3$ and Mn^{2+}:$CsPbCl_3$/Cs_4PbCl_6 core/shell NCs with Mn/Pb ratios of 2/1 are shown in Figure S7.

DOI: 10.1021/acs.jpcc.9b03294
J. Phys. Chem. C 2019, 123, 14849−14857

After coating the shell, the size of the NCs increases from 7.92 to 9.06 nm, indicating that the thickness of shell is 0.57 nm, and two new diffraction peaks at 13.4 and 27.0° are found, corresponding to (110) and (220) directions of Cs_4PbCl_6 structure (JCPDS: 76-1530), which demonstrates that the Cs_4PbCl_6 shell is successfully coated on the surface of the Mn^{2+}:$CsPbCl_3$ core. The absorption and PL spectra of Mn^{2+}:$CsPbCl_3$ and Mn^{2+}:$CsPbCl_3$/Cs_4PbCl_6 core/shell NCs with various Mn/Pb ratios in hexane are shown in Figure S8. The observation of a sharp absorption band near 350 nm confirms the successful coating of a Cs_4PbCl_6 shell on the Mn^{2+}:$CsPbCl_3$ core NCs.[66] Figure 7 shows the PL spectra and

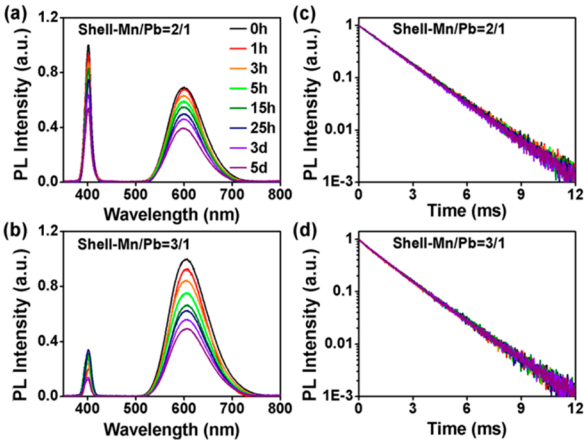

Figure 7. PL spectra of Mn^{2+}:$CsPbCl_3$/Cs_4PbCl_6 core/shell NCs with Mn/Pb ratios of 2/1 (a) and 3/1 (b) and the corresponding Mn^{2+} PL decay curves (c, d) under various illumination times.

decay curves of Mn^{2+}:$CsPbCl_3$/Cs_4PbCl_6 core/shell NCs under various illumination times. Only two Mn^{2+}:$CsPbCl_3$ NC films with Mn/Pb ratios of 2/1 and 3/1 as an example are provided to show relatively long and stable PL lifetimes of Mn^{2+} ions. As seen in Figure 7a and b, the relatively small reduction in PL intensities of band-edge excitons and Mn^{2+} ions is observed, compared with those of doped NCs without a shell as seen in Figure 5. It is clearly noted that the Mn^{2+}:$CsPbCl_3$/Cs_4PbCl_6 core/shell NCs with Mn/Pb ratios of 2/1 and 3/1 still have Mn^{2+} PL bands at 600 and 610 nm, respectively, while they do not show any blue-shift in Mn^{2+} PL after a long illumination time. However, the blue-shift of the Mn^{2+} PL band in Mn^{2+}:$CsPbCl_3$/Cs_4PbCl_6 core/shell NCs with the highest Mn/Pb ratio of 5/1 is also found as shown in Figure S9a, indicating that Mn^{2+} ions still escape from the doped NCs under illumination, perhaps due to unsuccessful shell coating. As seen in Figures 7c and d and S9b, the PL lifetimes of Mn^{2+} ions are 1.75 ± 0.02, 1.66 ± 0.03, and 1.01 ± 0.07 ms, respectively, for Mn^{2+}:$CsPbCl_3$/Cs_4PbCl_6 core/shell NCs with Mn/Pb ratios of 2/1, 3/1, and 5/1 under various illumination times. On the other hand, the PL decay curves of Mn^{2+} ions in Mn^{2+}:$CsPbCl_3$/Cs_4PbCl_6 core/shell NCs in solutions and films with various Mn/Pb ratios at different emission wavelengths were also measured, as shown in Figures S10 and S11, respectively. The PL lifetimes of Mn^{2+} ions in $CsPbCl_3$/Cs_4PbCl_6 core/shell NC films with various Mn/Pb ratios of 1/1, 2/1, 3/1, and 5/1 at different emission wavelengths have a slight reduction, compared with the core/shell NCs in solution. The PL lifetimes of Mn^{2+} emissions at their peak wavelengths are 1.80 ± 0.02, 1.79 ± 0.01, 1.76 ± 0.01, and 1.18 ± 0.05 ms for NC solution and 1.62 ± 0.01, 1.69 ± 0.01, 1.60 ± 0.04, and 0.93 ± 0.06 ms for NC films, respectively. The Mn^{2+}:$CsPbCl_3$/Cs_4PbCl_6 core/shell NCs clearly show much more significantly increased Mn^{2+} lifetimes than those in the naked ones, indicating that the Cs_4PbCl_6 shell effectively improves the photostability of Mn^{2+} doped $CsPbCl_3$ NCs.

Upon the illumination effect, the UV light-induced degradation of luminescence in Mn^{2+}:$CsPbCl_3$ NCs can be explained by the formation of nonradiative defects/traps due to the photo-oxidation of the doped NCs. The light-induced degradation in $CsPbBr_3$ NCs under high-power LED illumination was related to oxygen-induced degradation and increased surface trap states due to growth of NCs.[42] The light-induced degradation in yellow-emitting K_2SiF_6:Mn^{2+} phosphors was attributed to photo-oxidation of Mn^{2+} to Mn^{2+} and formation of nonradiative defects/traps in NCs.[67] Recently, the light-induced photophysical variation in organic metal halide perovskites in the presence of oxygen was explained by light-induced ion migration.[41] Also recently, the oxygen-induced performance degradation of Mn^{2+} emission including PL intensity and lifetime was observed in Mn^{2+}:$CsPbCl_3$ NCs.[68] The significant reduction in PL lifetimes of Mn^{2+} ions was considered to be related to absorbed oxygen on the NC surface. In our experiment, the illumination-induced defect/traps in $CsPbCl_3$ host reduces the energy transfer from NC host to Mn^{2+} ions, only quenching the Mn^{2+} PL intensity. The PL lifetime of Mn^{2+} ions is unchanged because no efficient energy transfer occurs between Mn^{2+} ions and illumination-induced defect/traps in the NC hosts. Therefore, the Cs_4PbCl_6 shell significantly suppresses the UV light-induced degradation of luminescence in Mn^{2+}:$CsPbCl_3$ NCs.

4. CONCLUSIONS

In summary, the UV illumination effects on optical properties of Mn^{2+}:$CsPbCl_3$ core and Mn^{2+}:$CsPbCl_3$/Cs_4PbCl_6 core/shell NCs have been studied by steady-state and time-resolved PL spectroscopy. The UV illumination resulted in the formation of an amount of defect/trap states, degrading the PL properties of Mn^{2+}:$CsPbCl_3$ NCs by reducing PL intensities and lifetimes of band-edge excitons and by reducing PL intensities of Mn^{2+} ions but not by reducing PL lifetimes of Mn^{2+} ions. The unchanged single-exponential decay times of Mn^{2+} emissions in the doped NCs with low Mn/Pb ratios under various UV illumination times indicated that the local environment around Mn^{2+} ions is relative stable. The observation of Mn^{2+} emission blue-shift in high Mn^{2+} doping concentration NCs under illumination suggested the diffusion of Mn^{2+} ions out of doped NCs. The Cs_4PbCl_6 shell effectively passivated Mn^{2+}:$CsPbCl_3$ NCs, suppressed the UV light-induced degradation of Mn^{2+}:$CsPbCl_3$ NCs, and enhanced Mn^{2+} PL. In addition, the XRD patterns and TEM images clarified that there was no clear structural change and aggregated Pb atoms in illuminated Mn^{2+}:$CsPbCl_3$ NCs. Therefore, the metal doping and shell coating can effectively suppress photo-oxidation of Mn^{2+}:$CsPbCl_3$ NCs and the diffusion of Mn^{2+} out of doped NCs, further improving their photostability.

■ ASSOCIATED CONTENT

Supporting Information

The Supporting Information is available free of charge on the ACS Publications website at DOI: 10.1021/acs.jpcc.9b03294.

DOI: 10.1021/acs.jpcc.9b03294
J. Phys. Chem. C 2019, 123, 14849−14857

TEM images and XRD of the Mn^{2+}:$CsPbCl_3$ NCs; absorption, PL spectra, and decay curves of Mn^{2+}:$CsPbCl_3$ NCs and Mn^{2+}:$CsPbCl_3$/Cs_4PbCl_6 core/shell NCs (PDF)

AUTHOR INFORMATION

Corresponding Authors

*E-mail: yuanx@jlnu.edu.cn.

*E-mail: lihaibo@jlnu.edu.cn.

ORCID

Xi Yuan: 0000-0001-8731-216X

Yi Fan: 0000-0003-0379-9842

Jialong Zhao: 0000-0001-9020-1436

Haibo Li: 0000-0001-6108-1965

Notes

The authors declare no competing financial interest.

ACKNOWLEDGMENTS

This work was supported by the National Natural Science Foundation of China (11704152, 11774134, and 21371071), Development of Science and Technology of Jilin Province (20190302084GX), and the Thirteenth Five-Year Program for Science and Technology of Education Department of Jilin Province (JJKH20191002KJ).

REFERENCES

(1) Protesescu, L.; Yakunin, S.; Bodnarchuk, M. I.; Krieg, F.; Caputo, R.; Hendon, C. H.; Yang, R. X.; Walsh, A.; Kovalenko, M. V. Nanocrystals of Cesium Lead Halide Perovskites ($CsPbX_3$, X = Cl, Br, and I): Novel Optoelectronic Materials Showing Bright Emission with Wide Color Gamut. *Nano Lett.* **2015**, *15*, 3692−3696.

(2) Kovalenko, M. V.; Protesescu, L.; Bodnarchuk, M. I. Properties and Potential Optoelectronic Applications of Lead Halide Perovskite Nanocrystals. *Science* **2017**, *358*, 745−750.

(3) Akkerman, Q. A.; Raino, G.; Kovalenko, M. V.; Manna, L. Genesis, Challenges and Opportunities for Colloidal Lead Halide Perovskite Nanocrystals. *Nat. Mater.* **2018**, *17*, 394−405.

(4) Wei, Y.; Cheng, Z. Y.; Lin, J. An Overview on Enhancing the Stability of Lead Halide Perovskite Quantum Dots and Their Applications in Phosphor-Converted LEDs. *Chem. Soc. Rev.* **2019**, *48*, 310−350.

(5) Shamsi, J.; Urban, A. S.; Imran, M.; De Trizio, L.; Manna, L. Metal Halide Perovskite Nanocrystals: Synthesis, Post-Synthesis Modifications, and Their Optical Properties. *Chem. Rev.* **2019**, *119*, 3296−3348.

(6) Akkerman, Q. A.; Gandini, M.; Di Stasio, F.; Rastogi, P.; Palazon, F.; Bertoni, G.; Ball, J. M.; Prato, M.; Petrozza, A.; Manna, L. Strongly Emissive Perovskite Nanocrystal Inks for High-Voltage Solar Cells. *Nat. Energy* **2017**, *2*, 16194.

(7) Song, J.; Li, J.; Li, X.; Xu, L.; Dong, Y.; Zeng, H. Quantum Dot Light-Emitting Diodes Based on Inorganic Perovskite Cesium Lead Halides ($CsPbX_3$). *Adv. Mater.* **2015**, *27*, 7162−7167.

(8) Li, X.; Wu, Y.; Zhang, S.; Cai, B.; Gu, Y.; Song, J.; Zeng, H. $CsPbX_3$ Quantum Dots for Lighting and Displays: Room-Temperature Synthesis, Photoluminescence Superiorities, Underlying Origins and White Light-Emitting Diodes. *Adv. Funct. Mater.* **2016**, *26*, 2435−2445.

(9) Li, J.; et al. 50-Fold Eqe Improvement up to 6.27% of Solution-Processed All-Inorganic Perovskite $CsPbBr_3$ QLEDs via Surface Ligand Density Control. *Adv. Mater.* **2017**, *29*, 1603885.

(10) Song, J.; Li, J.; Xu, L.; Li, J.; Zhang, F.; Han, B.; Shan, Q.; Zeng, H. Room-Temperature Triple-Ligand Surface Engineering Synergistically Boosts Ink Stability, Recombination Dynamics, and Charge Injection toward EQE-11.6% Perovskite QLEDs. *Adv. Mater.* **2018**, *30*, 1800764.

(11) Yakunin, S.; Protesescu, L.; Krieg, F.; Bodnarchuk, M. I.; Nedelcu, G.; Humer, M.; De Luca, G.; Fiebig, M.; Heiss, W.; Kovalenko, M. V. Low-Threshold Amplified Spontaneous Emission and Lasing from Colloidal Nanocrystals of Caesium Lead Halide Perovskites. *Nat. Commun.* **2015**, *6*, 8056.

(12) Wang, Y.; Li, X.; Song, J.; Xiao, L.; Zeng, H.; Sun, H. All-Inorganic Colloidal Perovskite Quantum Dots: A New Class of Lasing Materials with Favorable Characteristics. *Adv. Mater.* **2015**, *27*, 7101−7108.

(13) Swarnkar, A.; Marshall, A. R.; Sanehira, E. M.; Chernomordik, B. D.; Moore, D. T.; Christians, J. A.; Chakrabarti, T.; Luther, J. M. Quantum Dot−Induced Phase Stabilization of A-$CsPbI_3$ Perovskite for High-Efficiency Photovoltaics. *Science* **2016**, *354*, 92−95.

(14) Parobek, D.; Roman, B. J.; Dong, Y. T.; Jin, H.; Lee, E.; Sheldon, M.; Son, D. H. Exciton-to-Dopant Energy Transfer in Mn-Doped Cesium Lead Halide Perovskite Nanocrystals. *Nano Lett.* **2016**, *16*, 7376−7380.

(15) Liu, W. Y.; Lin, Q. L.; Li, H. B.; Wu, K. F.; Robel, I.; Pietryga, J. M.; Klimov, V. I. Mn^{2+}-Doped Lead Halide Perovskite Nanocrystals with Dual-Color Emission Controlled by Halide Content. *J. Am. Chem. Soc.* **2016**, *138*, 14954−14961.

(16) Liu, H. W.; Wu, Z. N.; Shao, J. R.; Yao, D.; Gao, H.; Liu, Y.; Yu, W. L.; Zhang, H.; Yang, B. $CsPb_XMn_{1-X}Cl_3$ Perovskite Quantum Dots with High Mn Substitution Ratio. *ACS Nano* **2017**, *11*, 2239−2247.

(17) Lin, C. C.; Xu, K. Y.; Wang, D.; Meijerink, A. Luminescent Manganese-Doped $CsPbCl_3$ Perovskite Quantum Dots. *Sci. Rep.* **2017**, *7*, 45906.

(18) Guria, A. K.; Dutta, S. K.; Das Adhikari, S.; Pradhan, N. Doping Mn^{2+} in Lead Halide Perovskite Nanocrystals: Successes and Challenges. *ACS Energy Lett.* **2017**, *2*, 1014−1021.

(19) Das Adhikari, S.; Dutta, S. K.; Dutta, A.; Guria, A. K.; Pradhan, N. Chemically Tailoring the Dopant Emission in Manganese-Doped $CsPbCl_3$ Perovskite Nanocrystals. *Angew. Chem., Int. Ed.* **2017**, *56*, 8746−8750.

(20) Huang, G.; Wang, C.; Xu, S.; Zong, S.; Lu, J.; Wang, Z.; Lu, C.; Cui, Y. Postsynthetic Doping of $MnCl_2$ Molecules into Preformed $CsPbBr_3$ Perovskite Nanocrystals Via a Halide Exchange-Driven Cation Exchange. *Adv. Mater.* **2017**, *29*, 1700095.

(21) Xu, K.; Lin, C. C.; Xie, X.; Meijerink, A. Efficient and Stable Luminescence from Mn^{2+} in Core and Core-Isocrystalline Shell $CsPbCl_3$ Perovskite Nanocrystals. *Chem. Mater.* **2017**, *29*, 4265−4272.

(22) Rossi, D.; Parobek, D.; Dong, Y.; Son, D. H. Dynamics of Exciton-Mn Energy Transfer in Mn-Doped $CsPbCl_3$ Perovskite Nanocrystals. *J. Phys. Chem. C* **2017**, *121*, 17143−17149.

(23) Yuan, X.; Ji, S. H.; De Siena, M. C.; Fei, L. L.; Zhao, Z.; Wang, Y. J.; Li, H. B.; Zhao, J. L.; Gamelin, D. R. Photoluminescence Temperature Dependence, Dynamics, and Quantum Efficiencies in Mn^{2+}-Doped $CsPbCl_3$ Perovskite Nanocrystals with Varied Dopant Concentration. *Chem. Mater.* **2017**, *29*, 8003−8011.

(24) De, A.; Mondal, N.; Samanta, A. Luminescence Tuning and Exciton Dynamics of Mn-Doped $CsPbCl_3$ Nanocrystals. *Nanoscale* **2017**, *9*, 16722−16727.

(25) Zhu, J.; Yang, X.; Zhu, Y.; Wang, Y.; Cai, J.; Shen, J.; Sun, L.; Li, C. Room-Temperature Synthesis of Mn-Doped Cesium Lead Halide Quantum Dots with High Mn Substitution Ratio. *J. Phys. Chem. Lett.* **2017**, *8*, 4167−4171.

(26) Wei, Q.; Li, M.; Zhang, Z.; Guo, J.; Xing, G.; Sum, T. C.; Huang, W. Efficient Recycling of Trapped Energies for Dual-Emission in Mn-Doped Perovskite Nanocrystals. *Nano Energy* **2018**, *51*, 704−710.

(27) Pinchetti, V.; Anand, A.; Akkerman, Q. A.; Sciacca, D.; Lorenzon, M.; Meinardi, F.; Fanciulli, M.; Manna, L.; Brovelli, S. Trap-Mediated Two-Step Sensitization of Manganese Dopants in Perovskite Nanocrystals. *ACS Energy Lett.* **2019**, *4*, 85−93.

(28) Xu, K.; Meijerink, A. Tuning Exciton-Mn^{2+} Energy Transfer in Mixed Halide Perovskite Nanocrystals. *Chem. Mater.* **2018**, *30*, 5346−5352.

DOI: 10.1021/acs.jpcc.9b03294
J. Phys. Chem. C 2019, 123, 14849−14857

(29) Fei, L.; Yuan, X.; Hua, J.; Ikezawa, M.; Zeng, R.; Li, H.; Masumoto, Y.; Zhao, J. Enhanced Luminescence and Energy Transfer in Mn^{2+} Doped $CsPbCl_{3-x}Br_x$ Perovskite Nanocrystals. *Nanoscale* **2018**, *10*, 19435−19442.
(30) Chen, D.; Fang, G.; Chen, X. Silica-Coated Mn-Doped $CsPb(Cl/Br)_3$ Inorganic Perovskite Quantum Dots: Exciton-to-Mn Energy Transfer and Blue-Excitable Solid-State Lighting. *ACS Appl. Mater. Interfaces* **2017**, *9*, 40477−40487.
(31) Chen, W.; Shi, T.; Du, J.; Zang, Z.; Yao, Z.; Li, M.; Sun, K.; Hu, W.; Leng, Y.; Tang, X. Highly Stable Silica-Wrapped Mn-Doped $CsPbPl_3$ Quantum Dots for Bright White Light-Emitting Devices. *ACS Appl. Mater. Interfaces* **2018**, *10*, 43978−43986.
(32) Ye, S.; Sun, J.-Y.; Han, Y.-H.; Zhou, Y.-Y.; Zhang, Q.-Y. Confining Mn2+-Doped Lead Halide Perovskite in Zeolite-Y as Ultrastable Orange-Red Phosphor Composites for White Light-Emitting Diodes. *ACS Appl. Mater. Interfaces* **2018**, *10*, 24656−24664.
(33) He, M.; Cheng, Y.; Shen, L.; Shen, C.; Zhang, H.; Xiang, W.; Liang, X. Mn-Doped $CsPbCl_3$ Perovskite Quantum Dots (PQDs) Incorporated into Silica/Alumina Particles Used for WLEDs. *Appl. Surf. Sci.* **2018**, *448*, 400−406.
(34) Bryant, D.; Aristidou, N.; Pont, S.; Sanchez-Molina, I.; Chotchunangatchaval, T.; Wheeler, S.; Durrant, J. R.; Haque, S. A. Light and Oxygen Induced Degradation Limits the Operational Stability of Methylammonium Lead Triiodide Perovskite Solar Cells. *Energy Environ. Sci.* **2016**, *9*, 1655−1660.
(35) Manser, J. S.; Saidaminov, M. I.; Christians, J. A.; Bakr, O. M.; Kamat, P. V. Making and Breaking of Lead Halide Perovskites. *Acc. Chem. Res.* **2016**, *49*, 330−338.
(36) Divitini, G.; Cacovich, S.; Matteocci, F.; Cina, L.; Di Carlo, A.; Ducati, C. In Situ Observation of Heat-Induced Degradation of Perovskite Solar Cells. *Nat. Energy* **2016**, *1*, 15012.
(37) Nickel, N. H.; Lang, F.; Brus, V. V.; Shargaieva, O.; Rappich, J. Unraveling the Light-Induced Degradation Mechanisms of $CH_3NH_3PBI_3$ Perovskite Films. *Adv. Electron. Mater.* **2017**, *3*, 1700158.
(38) Abdelmageed, G.; Jewell, L.; Hellier, K.; Seymour, L.; Luo, B.; Bridges, F.; Zhang, J. Z.; Carter, S. Mechanisms for Light Induced Degradation in $MAPbI_3$ Perovskite Thin Films and Solar Cells. *Appl. Phys. Lett.* **2016**, *109*, 233905.
(39) Xu, R.-P.; Li, Y.-Q.; Jin, T.-Y.; Liu, Y.-Q.; Bao, Q.-Y.; O'Carroll, C.; Tang, J.-X. In Situ Observation of Light Illumination-Induced Degradation in Organometal Mixed-Halide Perovskite Films. *ACS Appl. Mater. Interfaces* **2018**, *10*, 6737−6746.
(40) Li, Y.; Xu, X.; Wang, C.; Ecker, B.; Yang, J.; Huang, J.; Gao, Y. Light-Induced Degradation of $CH_3NH_3PbI_3$ Hybrid Perovskite Thin Film. *J. Phys. Chem. C* **2017**, *121*, 3904−3910.
(41) Anaya, M.; Galisteo-Lopez, J. F.; Calvo, M. E.; Espinos, J. P.; Miguez, H. Origin of Light-Induced Photophysical Effects in Organic Metal Halide Perovskites in the Presence of Oxygen. *J. Phys. Chem. Lett.* **2018**, *9*, 3891−3896.
(42) Huang, S.; Li, Z.; Wang, B.; Zhu, N.; Zhang, C.; Kong, L.; Zhang, Q.; Shan, A.; Li, L. Morphology Evolution and Degradation of $CsPbBr_3$ Nanocrystals under Blue Light-Emitting Diode Illumination. *ACS Appl. Mater. Interfaces* **2017**, *9*, 7249−7258.
(43) An, R.; et al. Photostability and Photodegradation Processes in Colloidal $CsPbI_3$ Perovskite Quantum Dots. *ACS Appl. Mater. Interfaces* **2018**, *10*, 39222−39227.
(44) Pan, G.; et al. Doping Lanthanide into Perovskite Nanocrystals: Highly Improved and Expanded Optical Properties. *Nano Lett.* **2017**, *17*, 8005−8011.
(45) Milstein, T. J.; Kroupa, D. M.; Gamelin, D. R. Picosecond Quantum Cutting Generates Photoluminescence Quantum Yields over 100% in Ytterbium-Doped $CsPbCl_3$ Nanocrystals. *Nano Lett.* **2018**, *18*, 3792−3799.
(46) Liu, Y.; Pan, G.; Wang, R.; Shao, H.; Wang, H.; Xu, W.; Cui, H.; Song, H. Considerably Enhanced Exciton Emission of $CsPbCl_3$ Perovskite Quantum Dots by the Introduction of Potassium and Lanthanide Ions. *Nanoscale* **2018**, *10*, 14067−14072.
(47) Ahmed, G. H.; El-Demellawi, J. K.; Yin, J.; Pan, J.; Velusamy, D. B.; Hedhili, M. N.; Alarousu, E.; Bakr, O. M.; Alshareef, H. N.; Mohammed, O. F. Giant Photoluminescence Enhancement in $CsPbCl_3$ Perovskite Nanocrystals by Simultaneous Dual-Surface Passivation. *ACS Energy Lett.* **2018**, *3*, 2301−2307.
(48) Behera, R. K.; Das Adhikari, S.; Dutta, S. K.; Dutta, A.; Pradhan, N. Blue-Emitting $CsPbCl_3$ Nanocrystals: Impact of Surface Passivation for Unprecedented Enhancement and Loss of Optical Emission. *J. Phys. Chem. Lett.* **2018**, *9*, 6884−6891.
(49) Mondal, N.; De, A.; Samanta, A. Achieving near-Unity Photoluminescence Efficiency for Blue-Violet-Emitting Perovskite Nanocrystals. *ACS Energy Lett.* **2019**, *4*, 32−39.
(50) Zhai, Y.; Bai, X.; Pan, G.; Zhu, J.; Shao, H.; Dong, B.; Xu, L.; Song, H. Effective Blue-Violet Photoluminescence through Lanthanum and Fluorine Ions Co-Doping for $CsPbCl_3$ Perovskite Quantum Dots. *Nanoscale* **2019**, *11*, 2484−2491.
(51) Yong, Z.-J.; et al. Doping-Enhanced Short-Range Order of Perovskite Nanocrystals for near-Unity Violet Luminescence Quantum Yield. *J. Am. Chem. Soc.* **2018**, *140*, 9942−9951.
(52) Wu, Y.; Li, X.; Zeng, H. Highly Luminescent and Stable Halide Perovskite Nanocrystals. *ACS Energy Lett.* **2019**, *4*, 673−681.
(53) Zou, S.; et al. Stabilizing Cesium Lead Halide Perovskite Lattice through Mn(II) Substitution for Air-Stable Light-Emitting Diodes. *J. Am. Chem. Soc.* **2017**, *139*, 11443−11450.
(54) Akkerman, Q. A.; Meggiolaro, D.; Dang, Z. Y.; De Angelis, F.; Manna, L. Fluorescent Alloy $CsPb_xMn_{1-x}I_3$ Perovskite Nanocrystals with High Structural and Optica Stability. *ACS Energy Lett.* **2017**, *2*, 2183−2186.
(55) Swarnkar, A.; Mir, W. J.; Nag, A. Can B-Site Doping or Alloying Improve Thermal- and Phase-Stability of All-Inorganic $CsPbX_3$ (X = Cl, Br, I) Perovskites? *ACS Energy Lett.* **2018**, *3*, 286−289.
(56) Luo, B.; Li, F.; Xu, K.; Guo, Y.; Liu, Y.; Xia, Z.; Zhang, J. Z. B-Site Doped Lead Halide Perovskites: Synthesis, Band Engineering, Photophysics, and Light Emission Applications. *J. Mater. Chem. C* **2019**, *7*, 2781−2808.
(57) Zhou, Y.; Chen, J.; Bakr, O. M.; Sun, H.-T. Metal-Doped Lead Halide Perovskites: Synthesis, Properties, and Optoelectronic Applications. *Chem. Mater.* **2018**, *30*, 6589−6613.
(58) Ji, S.; Yuan, X.; Li, J.; Hua, J.; Wang, Y.; Zeng, R.; Li, H.; Zhao, J. Photoluminescence Lifetimes and Thermal Degradation of Mn^{2+}-Doped $CsPbCl_3$ Perovskite Nanocrystals. *J. Phys. Chem. C* **2018**, *122*, 23217−23223.
(59) Lakowicz, J. R. *Principles of Fluorescence Spectroscopy*, 3rd ed.; Springer-Verlag: Berlin, Germany, 2006.
(60) Yuan, X.; Hou, X.; Li, J.; Qu, C.; Zhang, W.; Zhao, J.; Li, H. Thermal Degradation of Luminescence in Inorganic Perovskite $CsPbBr_3$ Nanocrystals. *Phys. Chem. Chem. Phys.* **2017**, *19*, 8934−8940.
(61) Ma, J.; Yao, Q.; McLeod, J. A.; Chang, L.-Y.; Pao, C.-W.; Chen, J.; Sham, T.-K.; Liu, L. Investigating the Luminescence Mechanism of Mn-Doped $CsPb(Br/Cl)_3$ Nanocrystals. *Nanoscale* **2019**, *11*, 6182−6191.
(62) Moroz, P.; Royo Romero, L.; Zamkov, M. Colloidal Semiconductor Nanocrystals in Energy Transfer Reactions. *Chem. Commun.* **2019**, *55*, 3033−3048.
(63) Zhang, J.-C.; Zhao, L.-Z.; Long, Y.-Z.; Zhang, H.-D.; Sun, B.; Han, W.-P.; Yan, X.; Wang, X. Color Manipulation of Intense Multiluminescence from CaZnOS:Mn^{2+} by Mn^{2+} Concentration Effect. *Chem. Mater.* **2015**, *27*, 7481−7489.
(64) Zhou, Q.; Dolgov, L.; Srivastava, A. M.; Zhou, L.; Wang, Z.; Shi, J.; Dramicanin, M. D.; Brik, M. G.; Wu, M. Mn^{2+} and Mn^{4+} Red Phosphors: Synthesis, Luminescence and Applications in WLEDs. A Review. *J. Mater. Chem. C* **2018**, *6*, 2652−2671.
(65) Shi, L.; Huang, Y.; Seo, H. J. Emission Red Shift and Unusual Band Narrowing of Mn^{2+} in $NaCaPO_4$ Phosphor. *J. Phys. Chem. A* **2010**, *114*, 6927−6934.
(66) Jia, C.; Li, H.; Meng, X.; Li, H. $CsPbX_3/Cs_4PbX_6$ Core/Shell Perovskite Nanocrystals. *Chem. Commun.* **2018**, *54*, 6300−6303.

DOI: 10.1021/acs.jpcc.9b03294
J. Phys. Chem. C 2019, 123, 14849−14857

(67) Oyama, T.; Adachi, S. Unique Light-Induced Degradation in Yellow-Emitting $K_2SiF_6:Mn^{2+}$ Phosphor. *J. Appl. Phys.* **2014**, *116*, 133515.
(68) Lin, F.; Li, F.; Lai, Z.; Cai, Z.; Wang, Y.; Wolfbeis, O. S.; Chen, X. Mn-II-Doped Cesium Lead Chloride Perovskite Nanocrystals: Demonstration of Oxygen Sensing Capability Based on Luminescent Dopants and Host-Dopant Energy Transfer. *ACS Appl. Mater. Interfaces* **2018**, *10*, 23335−23343.

DOI: 10.1021/acs.jpcc.9b03294
J. Phys. Chem. C 2019, 123, 14849−14857